Integrated dynamic modeling of a shipborne multiple rocket launcher considering actuation torques

Pham Cong Dinh[1*], Nguyen Trang Minh[2], Nguyen Thanh Tien[3], Bui Dinh Tan[1]

[1]Institute of Missile, Academy of Military Science and Technology, 17 Hoang Sam, Nghia Do, Hanoi, Vietnam;
[2]Academy of Military Science and Technology, 17 Hoang Sam, Nghia Do, Hanoi, Vietnam;
[3]Institute of Military Vehicle Engineering, 42 Dong Quan, Nghia Do, Hanoi, Vietnam.
[*]Corresponding author: phamcongdinh2017@gmail.com
Received 24 Jun. 2026; Revised 16 Aug. 2026; Accepted 04 Sep. 2026; Published 16 Sep. 2026.
DOI: https://doi.org/10.54939/1859-1043.j.mst.FMC.2026.61-69

ABSTRACT

This paper develops an integrated dynamic model for a multiple rocket launcher (MRL) mounted on a floating platform (FP) and evaluates the model's structural consistency and computational feasibility through numerical simulations. The system is represented by five rigid bodies with a total of 11 degrees of freedom (DOFs). The 6-degree-of-freedom (6-DOF) dynamics of the FP are formulated using the Newton-Euler equations in a body-fixed reference frame, while the launcher subsystem, with five DOFs, is described by Lagrange's equations of the second kind in terms of generalized coordinates. The two formulations are coupled through the kinematic relations at the launcher mounting location and the corresponding interaction force-moment system. This hybrid formulation preserves the hydrodynamic structure of the FP model while providing a convenient representation of the launcher as a multibody chain. The model incorporates elastic-damping connections, environmental loads, launch loads, azimuth and elevation actuation torques, and an equivalent rocket package whose mass and inertia properties are updated according to firing events. The model is implemented in MATLAB, numerically integrated using the ode15s solver, and evaluated according to a PASS1-PASS2-PASS3 computational scheme. For the representative VH6-MTW7-KC4-DK4 scenario, the maximum roll angle of the FP decreases from 2.604° in PASS1 to 2.519° in PASS3, while the azimuth and elevation tracking errors remain bounded within the prescribed ±1° limit. The calculations involving the actuation torques, rocket-package updates, and sea-state variation are employed only to verify the functionality of the corresponding model components rather than to investigate in detail the individual influence of each factor. The results demonstrate that the proposed model is structurally consistent and computationally feasible. Parameter calibration and validation against experimental measurement data are identified as the next steps of the study.

Keywords: Multiple rocket launcher; Rocket projectile; Floating platform; Integrated dynamics; Vessel-launcher coupling; Numerical simulation.

1. INTRODUCTION

A multiple rocket launcher (MRL) mounted on a floating platform (FP) is simultaneously subjected to the platform's 6-DOF motion, wave-wind-current loads, and launch loads. For unguided rockets, even a small deviation in the launcher-tube axis orientation at the instant a rocket leaves the tube can alter the initial conditions of its trajectory; therefore, the platform motion, launcher response, and loads transmitted through the mounting interface must be described consistently [10-13].

Although the combined mass of the main launcher structural assemblies B2-B4 is only about 1.80 t, much smaller than the FP displacement of 919.76 t, an integrated model is still required to: (i) correctly transmit platform motion to the launcher-tube axis orientation; (ii) determine short-duration reactions at the pedestal base under launch loads and interface vibration; and (iii) quantify

launcher-to-vessel feedback to establish when two-way coupling may be neglected.

Previous studies have generally considered vessel dynamics or launcher dynamics separately [3, 4, 11]. Accordingly, this study focuses on developing an integrated vessel-launcher model and performing numerical trial runs to examine its consistency, coupling mechanism, and applicability. Actuation torques, rocket-package variation, and sea-state level are introduced as load/parameter branches required for model testing; detailed analysis of the influence of each factor, as well as the launcher control problem, is left for subsequent studies.

2. PROBLEM FORMULATION

2.1. Theoretical basis

2.1.1. Assumptions and multibody-system model

The system comprises vessel hull B1, support pedestal B2, azimuth assembly B3, elevation assembly B4, and the remaining rocket package B5. The vessel has 6 absolute coordinates $\boldsymbol{\eta} = [x_n, y_n, z_n, \varphi, \theta, \psi]^T$ in the {n} (NED) frame; the launcher has 5 relative coordinates $\mathbf{q} = [z_1, \varphi_1, \theta_1, \beta, \alpha]^T$ in the {b} (BODY) frame fixed to the vessel hull. The mechanical model and coordinate frames are shown in Figure 1.

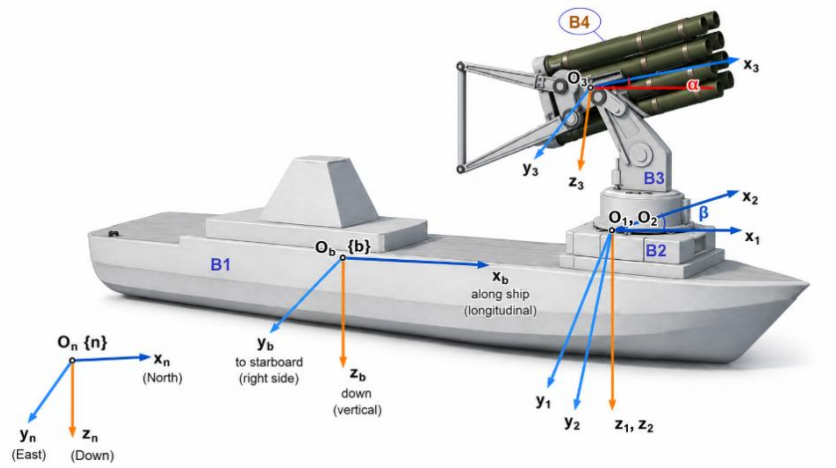


Figure 1. *Five-rigid-body mechanical model and coordinate frames of the FP-MRL system.*

The structural assemblies are treated as rigid bodies, except for the elastic-damping connection between the vessel deck and the support pedestal. The rocket package is not modeled as separate bodies; instead, it is represented by an equivalent body B5 with time-varying parameters, preserving the dominant effect of mass distribution while reducing model size [3, 4]. Figure 1 also defines the origin O_b of the vessel body-fixed frame and the origin O_1 of the support pedestal, which are used to establish the geometry of the vessel-launcher connection.

Given the mounting-position vector $\mathbf{r}^b_{O1/Ob}$, the kinematic relation between the vessel deck and support pedestal is described by the absolute position of O_1 and the pedestal orientation:

$$\mathbf{r}^n_{O1} = \mathbf{r}^n_{Ob} + \mathbf{R}^n_b(\boldsymbol{\eta})\left[\mathbf{r}^b_{O1/Ob} + (0,\ 0,\ z_1)^T\right]; \tag{1}$$

$$\mathbf{R}^n_1 = \mathbf{R}^n_b(\boldsymbol{\eta})\mathbf{R}_x(\varphi_1)\mathbf{R}_y(\theta_1). \tag{2}$$

The above relations provide a geometric mapping from the FP state and relative coordinates z_1, φ_1, θ_1 to the launcher pedestal state. These three coordinates define deformation of the elastic-damping interface and generate the corresponding generalized forces; the remaining constraint reactions at the pedestal base are recovered from equilibrium of the coupled equations and

included in $\boldsymbol{\tau}_{int}$ with opposite signs in the two subsystems. This treatment avoids inconsistency between the use of reaction forces in the Newton-Euler equations and the virtual-work principle in the Lagrange formulation.

2.1.2. Governing equations

The vessel kinematic relation in {n} is written as [5, 6]:

$$\dot{\boldsymbol{\eta}} = \mathbf{J}(\boldsymbol{\eta})\boldsymbol{\nu} \tag{3}$$

where $\boldsymbol{\eta}$ is the position-orientation vector, and $\boldsymbol{\nu}$ is the translational-angular velocity vector of the vessel expressed in {b}.

When current effects are included, the vessel relative velocity is defined as:

$$\boldsymbol{\nu}_{\mathrm{r}} = \boldsymbol{\nu} - \boldsymbol{\nu}_{\mathrm{c}} \tag{4}$$

where $\boldsymbol{\nu}_c$ is the current-velocity vector transformed into {b}. The 6-DOF vessel dynamics are then expressed in Newton-Euler form [6, 7]:

$$\mathbf{M}_T(\omega_{\mathrm{d}})\dot{\boldsymbol{\nu}}_r + [\mathbf{C}_{RB}(\boldsymbol{\nu}_r) + \mathbf{C}_A(\boldsymbol{\nu}_r, \omega_{\mathrm{d}})]\boldsymbol{\nu}_r + [\mathbf{B}(\omega_{\mathrm{d}}) + \mathbf{D}_V(\boldsymbol{\nu}_r)]\boldsymbol{\nu}_r + \mathbf{g}_T(\boldsymbol{\eta}) = \boldsymbol{\tau}_c + \boldsymbol{\tau}_{env} + \boldsymbol{\tau}_{int} \tag{5}$$

In the numerical implementation, (3) and (5) are integrated simultaneously using the state pair ($\boldsymbol{\eta}$, $\boldsymbol{\nu}$), consistent with the 6-DOF vessel model in the body-fixed frame {b} [5-7]. Equation (5) is not transformed entirely into a formulation in $\boldsymbol{\eta}$ because the hydrodynamic matrices $\mathbf{A}(\omega)$, $\mathbf{B}(\omega)$, Coriolis terms, and hydrodynamic loads are defined in {b}; $\boldsymbol{\eta}$ is updated directly from the kinematic equation (3).

The generalized mass matrix of the vessel is:

$$\mathbf{M}_T(\omega_{\mathrm{d}}) = \mathbf{M}_{RB} + \mathbf{A}(\omega_{\mathrm{d}}) \tag{6}$$

where $\boldsymbol{M}_T = \boldsymbol{M}_{RB} + \boldsymbol{A}(\omega_d)$; $\boldsymbol{C}_{RB}$ and $\boldsymbol{C}_A$ are the Coriolis matrices; $\boldsymbol{B}(\omega_d)$ and $\boldsymbol{D}_V$ are damping terms; $\boldsymbol{g}_T$ is the hydrostatic restoring vector; and $\boldsymbol{\tau}_c$, $\boldsymbol{\tau}_{env}$, and $\boldsymbol{\tau}_{int}$ are the control, environmental, and launcher-interaction loads, respectively. The matrices $\boldsymbol{A}(\omega_d)$ and $\boldsymbol{B}(\omega_d)$ are interpolated from frequency-domain hydrodynamic data computed using NEMOH [10].

Waves are represented by the JONSWAP spectrum, and the spectral peak frequency is used as the representative frequency for interpolating the hydrodynamic coefficients:

$$\omega_{\mathrm{d}} = \omega_p = \frac{2\pi}{T_p} \tag{7}$$

For the launcher subsystem, after defining the kinetic energy, potential energy, and Rayleigh dissipation function, Lagrange's equations of the second kind can be written as [2, 8]:

$$\mathbf{M}_g(\mathbf{q}, t)\,\ddot{\mathbf{q}} + \mathbf{h}_g(\mathbf{q}, \dot{\mathbf{q}}, \boldsymbol{\eta}, \boldsymbol{\nu}, \dot{\boldsymbol{\nu}}, t) = \mathbf{Q}_d + \mathbf{Q}_p \tag{8}$$

where $\boldsymbol{M}_g$ is the generalized mass matrix; $\boldsymbol{h}_g$ collects the Coriolis-centrifugal, gravitational, elastic-damping, and base-excitation terms; and $\boldsymbol{Q}_d$ and $\boldsymbol{Q}_p$ are the generalized forces due to actuation torques and launch loads, respectively.

In principle, the entire system could be formulated using Lagrange's equations of the second kind. However, using Newton-Euler equations for the FP and Lagrange's equations for the launcher preserves the conventional 6-DOF vessel structure and hydrodynamic coefficients defined in the body-fixed frame {b}, while generalized coordinates conveniently describe the launcher's multibody chain. The two subsystems share the same kinematic relations and obey an action-reaction force pair at the pedestal base; thus, this is a choice of representation and numerical implementation rather than two independent mechanical models.

The azimuth and elevation actuation torques enter the system directly as generalized forces:

$$\mathbf{Q}_d = \left[0,\ 0,\ 0,\ M_\beta(t),\ M_\alpha(t)\right]^T \tag{9}$$

where $M_\beta(t)$ and $M_\alpha(t)$ are treated as outputs of a reduced control-actuator subsystem that generates the actual torques at the two joints during model trial runs, thereby verifying that the $\boldsymbol{Q}_d$ branch is coupled correctly into the dynamic equations.

2.1.3. Time-varying mass-inertia model of the remaining rocket package

Let $S_c(t)$ denote the set of rockets remaining on the launcher at time t. The equivalent mass of the remaining rocket package is [4]:

$$m_c(t) = \sum_{i \in S_c(t)} m_i \tag{10}$$

The center-of-mass position and equivalent inertia tensor of this package are updated as:

$$\mathbf{r}_c(t) = \left(1/m_c(t)\right) \sum_{i \in S_c(t)} m_i\ \mathbf{r}_i \tag{11}$$

$$\mathbf{I}_c(t) = \sum_{i \in S_c(t)} \left[\mathbf{I}_i + m_i\left(\left(\boldsymbol{\rho}_i^T \boldsymbol{\rho}_i\right)\mathbf{E} - \boldsymbol{\rho}_i \boldsymbol{\rho}_i^T\right)\right] \tag{12}$$

where $\boldsymbol{r}_i$ and $\boldsymbol{I}_i$ are the position and inertia tensor of the ith rocket, respectively; $\boldsymbol{\rho}_i$ is the vector from the equivalent-package center of mass to the rocket center of mass. The quantities $m_c(t)$, $\boldsymbol{r}_c(t)$, and $\boldsymbol{I}_c(t)$ are updated immediately after each firing event.

2.2. Dynamic coupling between the vessel and launcher

The absolute velocities of the launcher bodies depend simultaneously on vessel motion and relative motion, so the total kinetic energy contains inertial coupling blocks. After separating the acceleration-dependent terms, the system can be written in block-matrix form:

$$\begin{bmatrix} \mathbf{M}_T & \mathbf{M}_{Tg} \\ \mathbf{M}_{gT} & \mathbf{M}_g \end{bmatrix} \begin{bmatrix} \dot{\mathbf{v}} \\ \ddot{q}_g \end{bmatrix} = \begin{bmatrix} \mathbf{R}_T \\ \mathbf{R}_g \end{bmatrix}. \tag{13}$$

where $\boldsymbol{M}_T$ and $\boldsymbol{M}_g$ are the vessel and launcher mass matrices; $\boldsymbol{M}_{Tg}$ and $\boldsymbol{M}_{gT}$ are the coupling blocks; and $\boldsymbol{R}_T$ and $\boldsymbol{R}_g$ contain loads independent of acceleration.

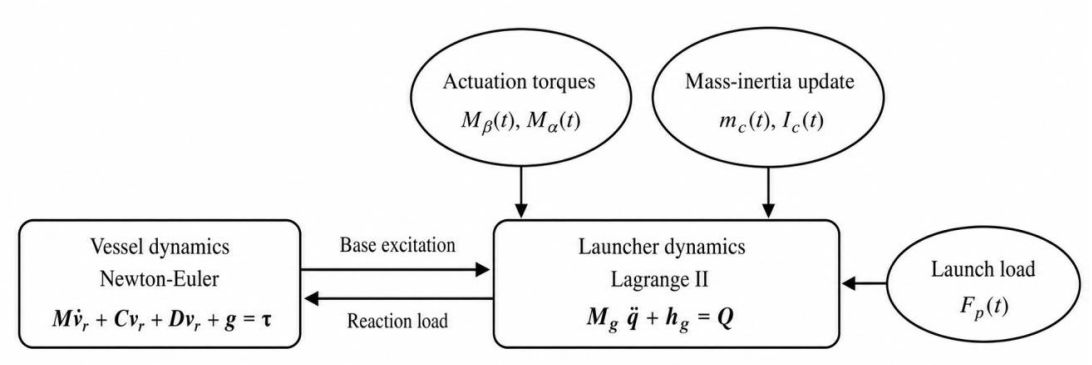


Figure 2. *Two-way coupling scheme among vessel dynamics, launcher dynamics, actuation torques, launch loads, and time-varying mass-inertia properties.*

The overall model is recast as a first-order state-space system [2, 5, 8]:

$$\dot{\mathbf{X}} = f\left(\mathbf{X}, t\right) \tag{14}$$

with the overall system state vector:

$$\mathbf{X} = \left[\boldsymbol{\eta}^T \quad \mathbf{v}^T \quad \mathbf{q}^T \quad \dot{\mathbf{q}}^T\right]^T \in \mathbb{R}^{22} \tag{15}$$

The system has 11 mechanical DOFs, corresponding to 22 first-order state variables, and is integrated using a stiff ODE solver.

2.3. Azimuth and elevation actuation torques

For model trial runs in a line-of-sight stabilization mode on a moving platform, the commanded line of sight defined in the NED frame is transformed into reference values for the azimuth and elevation joints; the corresponding actuation torques M_β and M_α are generated by the DK4 motion-compensating control structure. In this paper, DK4 serves only as a bounded test-torque source with saturation protection and a lock/brake function during firing; controller design, tuning, and optimization are beyond the main scope of this study.

2.4. Parameter setup for numerical trials

Table 1 summarizes the trial-scenario parameters and the principal characteristics of the system under study; detailed design data are not disclosed in this paper. For the environmental group in item 1, H_s and T_p define the JONSWAP spectrum, while the first-order wave loads are synthesized from frequency-domain wave-excitation forces computed by NEMOH using a finite-element model of the hull [10].

Table 1. *Simulation parameters and principal characteristics of the FP-MRL system.*

No.	Parameter group	Value setting	Role in model
1	Environment - MTW7	*JONSWAP: H_s = 1.2 m; T_p = 6 s; β_w = 90°; V_w = 10 m/s, β_g = 90°; V_c = 1 m/s, β_c = 90°.*	Representative environmental input for the trial scenario
2	Initial conditions	*T = 250 s; u_0 = 5 m/s; $\psi_0 = \psi_d$ = 0° NED.*	Initial state and time horizon
3	Launcher and target	*18 tubes; β_d = -45° (315°), α_d = 45° NED; tracking-error limit ±1°.*	Geometry and firing line of sight
4	Pedestal interface - KC4	*$K_x = K_y = 10^6$ N/m; $K_z = 2\times10^6$ N/m; $C_x = C_y = C_z = 2\times10^5$ N·s/m; $K_\varphi = K_\theta = 10^6$ N·m/rad; $C_\varphi = C_\theta = 2\times10^5$ N·m·s/rad.*	Elastic-damping properties and pedestal-base reactions
5	Firing scheme - VH6	*18 rounds in 3 salvos, 6 rockets per salvo; t_1 = 50 s; inter-shot interval 0.25 s; 60 s between salvo start times.*	Firing events and launch loads
6	Actuation torques - DK4	*Azimuth/elevation torque source with platform-motion compensation, torque limits, and lock/brake during firing.*	Excitation of the $\boldsymbol{Q}_d$ branch during trial runs
7	Rocket-package mass	*$m_c(t)$, $\mathbf{r}_c(t)$, $\mathbf{I}_c(t)$ updated after each firing; initial state: 18 rockets.*	Time-varying parameters over the firing sequence
8	Solver	*ode15s; segmented MaxStep 0.02/0.01/0.002 s; RelTol = 5×10^{-5}; AbsTol = 10^{-6}.*	Integration of the stiff ODE system

No.	Parameter group	Value setting	Role in model
Principal characteristics of the system under study			
9	Floating platform	*Displacement 919.76 t; L × B × T = 71.735 × 8.6 × 2.069 m; GM = 4.816 m;* $I_{xT} = 2.5\times10^{6}$, $I_{yT} = 9.6\times10^{5}$, $I_{zT} = 7.3\times10^{7}$ *kg·m².*	Vessel mass, hydrostatic, and inertia properties
10	Mounting location	$\mathbf{r}^{b}_{O1O\text{Ов}} = (12.997, -3.16, -3.5)\,\text{m}$	Vessel-launcher load-transfer lever arm
11	Launcher assemblies	$m_{B2} = 447$ *kg;* $m_{B3} = 608.3$ *kg;* $m_{B4} = 743$ *kg.*	Masses of bodies B2-B4
12	Rocket package B5	*18 rockets; mass per rocket 39.6 kg; inertia of one rocket diag(0.10, 3.25, 3.25) kg·m².*	Initial mass-inertia state

3. RESULTS AND DISCUSSION

3.1. Trial setup and evaluation criteria

The baseline scenario uses the VH6-MTW7-KC4-DK4 combination in Table 1 to activate the main model components simultaneously: platform motion, pedestal interface, launch loads, actuation torques, and rocket-package updating. The tracking command in the NED frame is $\beta_d = -45°$, $\alpha_d = 45°$; the firing schedule consists of three salvos, each containing six rounds. The primary model-evaluation criteria are boundedness of the solution, *roll, pitch,* and *heave* responses, correct timing of interaction loads, and azimuth-elevation tracking errors during the trial.

The model is implemented in MATLAB and integrated with ode15s. PASS1 determines the platform motion; PASS2 computes the launcher response and interaction loads; PASS3 updates the FP motion under the loads obtained from PASS2. The time grid is refined around firing instants; the tolerances and MaxStep settings are listed in Table 1.

3.2. Model consistency and stability checks

Before the baseline scenario is run, the model is checked in five categories: (i) matrix/vector dimensions and number of DOFs; (ii) symmetry, positive definiteness, and nonsingularity of the mass matrix; (iii) sign convention of interaction loads and completeness of pedestal-base reaction components; (iv) synchronization of firing events with updates of $m_c(t)$, $\mathbf{r}_c(t)$, $\mathbf{I}_c(t)$, and $\mathbf{Q}_p$; and (v) actual torque limits at the actuators. In the test cases performed, the solver produced bounded solutions without mass-matrix singularity or event-handling errors.

3.3. Integrated-model trial runs and response evaluation

The baseline MTW7-VH6-KC4-DK4 scenario is used to determine whether the two-way coupling mechanism produces physically consistent responses in both the FP and the launcher. Two illustrative quantities are selected: the vessel roll angle in PASS1 versus PASS3, and the azimuth-elevation tracking errors in the NED frame.

The peak |*roll*| decreases from *2.604°* in PASS1 to *2.519°* in PASS3 (approximately *3.3%*), while the RMS value decreases from *0.849°* to *0.788°* (approximately *7.1%*). The differences are concentrated around the firing salvos, indicating that the launcher interaction loads are fed back to the FP at the correct times but only modify the platform response locally. This result is consistent with the large mass disparity between the vessel and launcher: the influence of two-way coupling

on overall vessel motion is small but nonzero, and the model enables this influence to be quantified rather than assumed a priori.

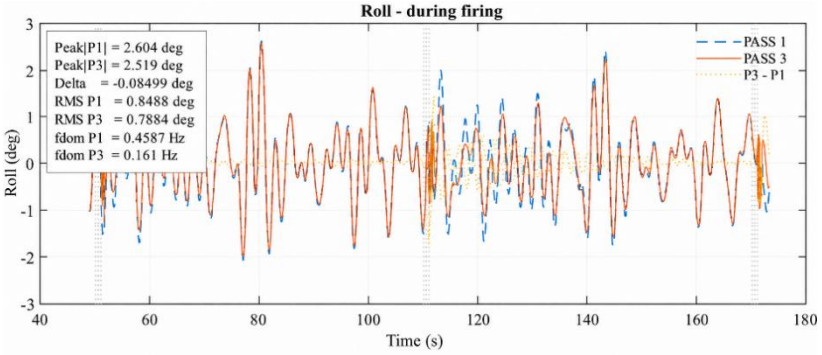


Figure 3. *Vessel roll response during the firing phase: PASS1 and PASS3.*

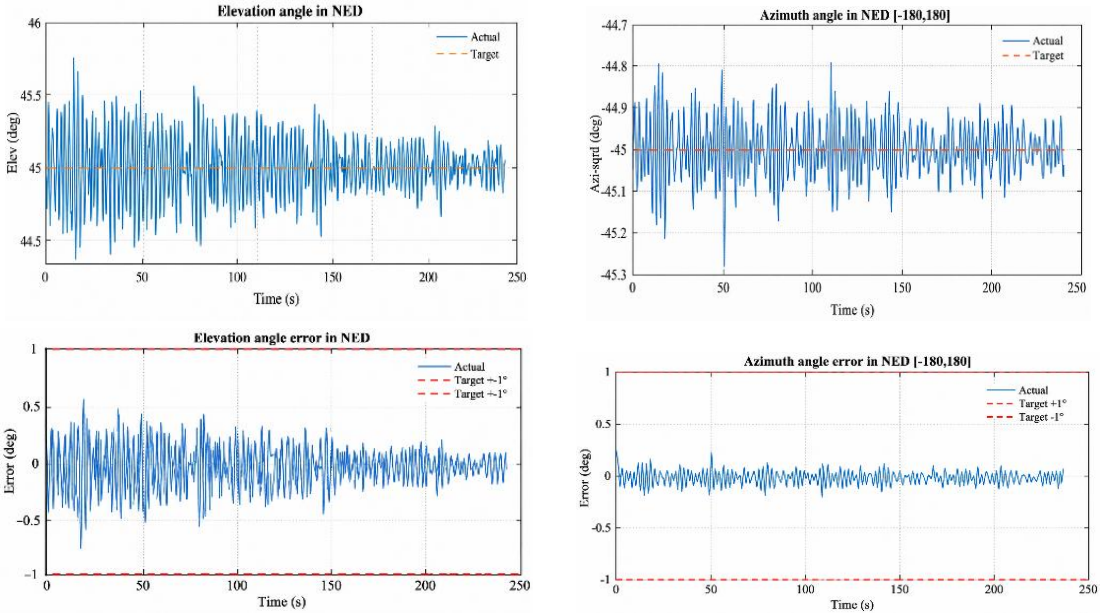


Figure 4. *Actual and commanded azimuth/elevation angles and tracking errors in the NED frame (β_d = -45°, α_d = 45°).*

Both channels track their setpoints with bounded oscillations; the largest errors occur during the transient phase and near firing instants but remain within the ±1° limit of the baseline scenario. This result serves as a functional check of the actuation-torque branch and the line-of-sight transformation.

3.4. Additional checks of model branches

Three auxiliary runs are retained strictly as functional checks. First, when the actuation torques are disabled/enabled, the maximum errors change from $e_{\alpha,max}$ = *2.49*° and $e_{\beta,max}$ = *2.06*° in DK1 to *0.75*° and *0.27*° in DK4, respectively, confirming that $\boldsymbol{Q}_d$ acts correctly on the elevation and azimuth coordinates. Second, updating B5 causes the number/mass of remaining rockets to decrease through *18-12-6-0*, with inertia parameters changing synchronously with firing events, confirming proper operation of the time-varying parameter branch. Third, representative wave cases over H_s = *0.4-2.0 m* all yield bounded solutions. This check is intended only to detect numerical instability. Detailed analyses of actuation-torque effects, mass-depletion laws, and sea-state effects will be addressed in separate studies.

4. CONCLUSIONS

This paper has developed an 11-DOF integrated dynamic model for the FP-MRL system, in which the Newton-Euler equations of the FP are coupled with Lagrange's equations of the second kind for the launcher through the kinematic relations at the mounting location and the interaction force-moment system. The two formulations are used to match the vessel hydrodynamic representation and the launcher generalized-coordinate structure; mechanically, the two subsystems belong to the same system and satisfy the action-reaction relation at the pedestal base.

Numerical trial results for the representative scenario show that the PASS1-PASS2-PASS3 scheme produces two-way feedback: peak $|roll|$ changes from $2.604°$ to $2.519°$ after the feedback update, while the azimuth and elevation channels remain bounded and keep their tracking errors within the prescribed $\pm 1°$ range. Checks of the matrices, firing events, torque limits, rocket-package updates, and investigated sea-state range reveal no signs of singularity or divergence. The model is therefore considered structurally sound and computationally feasible for studying vessel-launcher dynamics and for detailed investigation of factors affecting the dynamics of an MRL mounted on an FP.

The results concerning actuation torque, rocket-package variation, and sea state in this paper are used only to verify the respective model branches and are not intended to establish controller optimality or influence laws. Future work will focus on parameter calibration and validation against experimental measurements, followed by separate studies on control and on the effects of firing sequence, pedestal connection, and environmental conditions on system dynamics.

Acknowledgments: *The authors gratefully acknowledge the specialist units that provided design documentation and technical comments supporting completion of the model.*

REFERENCES

[1]. Nguyen Xuan Anh, *"Textbook on launcher calculations and launch dynamics,"* Military Technical Academy, Hanoi, (1998).

[2]. Nguyen Van Khang, *"Dynamics of multibody systems,"* Science and Technics Publishing House, Hanoi, (2007).

[3]. Pham Hong Sinh, *"Dynamic study of a launcher mounted on a wheeled vehicle,"* Ph.D. dissertation, Military Institute of Science and Technology, (2011).

[4]. Nguyen Duy Phon, *"Study on the influence of selected initial disturbances as an unguided rocket leaves the launcher on firing accuracy,"* Ph.D. dissertation, Military Technical Academy, (2017).

[5]. T. I. Fossen, *"Handbook of Marine Craft Hydrodynamics and Motion Control,"* John Wiley & Sons, (2011).

[6]. T. I. Fossen, *"Guidance and Control of Ocean Vehicles,"* John Wiley & Sons, 1994.

[7]. O. M. Faltinsen, *"Sea Loads on Ships and Offshore Structures,"* Cambridge University Press, (1990).

[8]. A. A. Shabana, *"Dynamics of Multibody Systems,"* 4th ed., Cambridge University Press, (2013).

[9]. L. F. Shampine and M. W. Reichelt, "*The MATLAB ODE Suite,*" SIAM Journal on Scientific Computing, vol. 18, no. 1, pp. 1-22, (1997).

[10]. A. Babarit and G. Delhommeau, "*Theoretical and numerical aspects of the open source BEM solver NEMOH,*" Proceedings of the 11th European Wave and Tidal Energy Conference, Nantes, France, (2015).

[11]. C. Yu, D. Ma, and X. Zhang, "*Launch process simulation of a ship-borne multiple launch rocket system,*" World Journal of Modelling and Simulation, vol. 3, no. 1, pp. 58–65, (2007).

[12]. Tran Xuan Dieu, *"Inverse kinematic analysis of a shipborne launcher model,"* Journal of Military Science and Technology, no. 80, (2022).

[13]. Le Tien Dung, *"Dynamics of a modified twin-barrel 37 mm gun mounted on a naval vessel and measures to ensure firing reliability,"* Ph.D. dissertation, Military Technical Academy, (2012).

TÓM TẮT

Mô hình động lực học tích hợp có xét mô men dẫn động cho giàn phóng đạn phản lực trên phương tiện nổi

Bài báo tập trung xây dựng mô hình động lực học tích hợp cho giàn phóng đạn phản lực (GPĐPL) trên phương tiện nổi (PTN) và đánh giá tính nhất quán, khả thi tính toán của mô hình bằng thử nghiệm số. Hệ được mô hình hóa bởi 5 vật rắn với 11 bậc tự do; động lực học 6 bậc tự do (6-DOF) của PTN được thiết lập theo Newton - Euler trong hệ tọa độ gắn thân PTN, còn phần giàn phóng với 5 bậc tự do được mô tả bằng phương trình Lagrange loại II theo các tọa độ suy rộng. Hai cách biểu diễn được ghép thông qua quan hệ động học tại vị trí lắp đặt và hệ lực - mô men tương tác, cho phép giữ cấu trúc thủy động lực học của PTN đồng thời mô tả thuận tiện chuỗi nhiều vật của giàn phóng. Mô hình xét liên kết đàn hồi - giảm chấn, tải môi trường, tải phóng, mô men dẫn động hướng - tầm và cụm đạn tương đương có các đặc trưng khối lượng - quán tính thay đổi theo sự kiện bắn. Mô hình được cài đặt trong MATLAB, tích phân bằng ode15s và chạy theo lược đồ PASS1 - PASS2 - PASS3. Với kịch bản đại diện VH6 - MTW7 - KC4 - DK4, góc lắc ngang (roll) lớn nhất của PTN thay đổi từ 2,604° ở PASS1 xuống 2,519° ở PASS3; sai số bám hướng - tầm hữu hạn và nằm trong giới hạn cài đặt ±1°. Việc tính toán đối với mô men dẫn động, cập nhật cụm đạn và mức sóng chỉ được dùng để kiểm tra chức năng của các thành phần mô hình, không nhằm khảo sát chi tiết ảnh hưởng của từng yếu tố. Kết quả cho thấy mô hình nhất quán về cấu trúc và khả thi về tính toán; việc hiệu chỉnh tham số và kiểm chứng bằng dữ liệu đo thực nghiệm được xác định là bước nghiên cứu tiếp theo.

Từ khóa: Giàn phóng; Đạn phản lực; Phương tiện nổi; Động lực học tích hợp; Ghép tàu - giàn; Thử nghiệm số.